

High-Pressure Synthesis of Metallic Perovskite Ruthenate $\text{CaCu}_3\text{Ga}_2\text{Ru}_2\text{O}_{12}$

Song-Ho Byeon,^{*,†} Seoung-Soo Lee,[†] John B. Parise,^{*,‡}
Patrick M. Woodward,[§] and Nam Hwi Hur^{||}

College of Environment and Applied Chemistry, Kyung Hee University,
Kyung Ki 449-701, Korea, Department of Geosciences and Mineral Physics Institute,
State University of New York, Stony Brook, New York 11794-2100, Department of Chemistry,
The Ohio State University, Columbus, Ohio 43210-1185, and Center for CMR Materials,
KRISS, Taejon 305-600, Korea

Received May 10, 2004. Revised Manuscript Received July 20, 2004

A new perovskite ruthenate, $\text{CaCu}_3\text{Ga}_2\text{Ru}_2\text{O}_{12}$, has been synthesized at 12.5 GPa and 1200 °C and recovered to room pressure and temperature conditions. This oxide is isostructural with $\text{CaCu}_3\text{Ti}_4\text{O}_{12}$ and $\text{CaCu}_3\text{Ru}_4\text{O}_{12}$, crystallizing in space group $\text{Im}\bar{3}$ with Ga and Ru cations disordered over the octahedral sites. $\text{CaCu}_3\text{Ga}_2\text{Ru}_2\text{O}_{12}$ exhibits a temperature-independent Pauli-paramagnetic and metallic character, indicating delocalized electrons for both Cu and Ru. Bond valence calculations based on the refined structure give oxidation states of 2.31 and 4.53 for copper and ruthenium cations, respectively. The itinerant electron behavior is thought to originate from a significant oxidation of Cu(II) by Ru(V). Such a situation corresponds to $\text{Cu}(\text{II})-\text{O}-\text{Ru}(\text{V}) \leftrightarrow \text{Cu}(\text{III})-\text{O}-\text{Ru}(\text{IV})$ valence degeneracy. This places $\text{CaCu}_3\text{Ga}_2\text{Ru}_2\text{O}_{12}$ among an unusual and interesting group of perovskites that show heteronuclear valence degeneracy.

Introduction

It is now accepted that the physicochemical properties in inorganic solids are coupled to the details of the crystal structure. In this respect ruthenates crystallizing in the perovskite-type structure have been extensively investigated for their structure–property relationships and for the correlations among structure, oxidation state of Ru, and transport properties. The ruthenates exhibit diverse magnetic and electrical properties depending on structural changes associated with ruthenium's tendency to readily adopt oxidation states of IV (d⁴) and V (d³) in oxides.

Both localized and itinerant electronic behaviors are frequently observed with perovskite-related oxides containing Ru(IV). For instance, SrRuO_3 shows a metallic and ferromagnetic behavior,¹ whereas CaRuO_3 has insulating and paramagnetic properties.^{2,3} This dramatic change in properties is ascribed to subtle differences in their crystal structures. The sensitivity to structural modifications is more profoundly demonstrated in the layered ruthenates. Remarkably, Sr_2RuO_4 is a noncuprate oxide superconductor,⁴ but strongly correlated Ca_2RuO_4 is a Mott insulator.⁵ Complex per-

ovskite-like ruthenates $\text{ACu}_3\text{Ru}_4\text{O}_{12}$ (A = Na, Ca, Ln) show metallic and Pauli-paramagnetic behavior.⁶

In contrast, insulating behavior and long-range magnetic order are generally observed for ruthenium(V) perovskite oxides, particularly those having the general formula A_2MRuO_6 and $\text{AA}'\text{MRuO}_6$, where A and A' are alkaline-earth metals or lanthanides and M is a transition metal or lanthanide. Although ferromagnetic or antiferromagnetic superexchange interactions are usually induced when M and Ru(V) cations are ordered,^{7–9} unusual magnetic properties are also observed when they are randomly distributed over the six-coordinate sites (the B-sites in the aristotype ABO_3 perovskite).¹⁰ For example, BaLaNiRuO_6 and $\text{Sr}_2\text{FeRuO}_6$ show spin-glass transitions.¹¹ $\text{Sr}_3\text{CaRu}_2\text{O}_9$ perovskite, which is characterized by a 2:1 ordering of Ru(V) and Ca(II) over the octahedral sites, is semiconducting, whereas the layered perovskite $\text{Sr}_{1.5}\text{Ca}_{0.5}\text{RuO}_4$, which is converted from $\text{Sr}_3\text{CaRu}_2\text{O}_9$ by heating in argon, is metallic.^{12,13}

⁵ Nakatsuji, S.; Ikeda, S.; Maeno, Y. *Physica C* **1997**, 282–287, 729.

⁶ Labeau, M.; Bochu, B.; Joubert, J. C.; Chenavas, J. *J. Solid State Chem.* **1980**, 33, 257.

⁷ Fernandez, I.; Greatrex, R.; Greenwood, N. N. *J. Solid State Chem.* **1980**, 32, 97.

⁸ Hayashi, K.; Demazeau, G.; Pouchard, M. *C. R. Acad. Sci.* **1981**, 292, 1433.

⁹ Battle, P. D.; Jones, C. W.; Studer, F. *J. Solid State Chem.* **1991**, 90, 302.

¹⁰ Woodward, P. M. Ph. D Dissertation, Oregon State University, Corvallis, OR, 1997.

¹¹ Battle, P. D.; Gibb, T. C.; Jones, C. W.; Studer, F. *J. Solid State Chem.* **1989**, 78, 281.

¹² Rijssenbeek, J. T.; Malo, S.; Caaignaert, V.; Poeppelmeier, K. R. *J. Am. Chem. Soc.* **2002**, 124, 2090.

¹³ Nakatsuji, S.; Ando, T.; Mao, Z.; Maeno, Y. *Physica B* **1999**, 261, 949.

* To whom correspondence should be addressed. E-mail: shbyun@knu.ac.kr (S.-H.B.); john.parise@sunysb.edu (J.B.P.).

[†] Kyung Hee University.

[‡] State University of New York.

[§] The Ohio State University.

^{||} KRISS.

(1) Kanbayashi, A. *J. Phys. Soc. Jpn.* **1976**, 41, 1876.

(2) Longo, J. M.; Raccah, P. M.; Goodenough, J. B. *J. Appl. Phys.* **1968**, 39, 1327.

(3) Yoshii, K.; Abe, H. *Physica B* **2002**, 312–313, 791.

(4) Maeno, Y.; Hashimoto, H.; Yoshida, K.; Nishizaki, S.; Fujita, T.; Bednorz, J. G.; Lichtenberg, F. *Nature* **1994**, 372, 532.

In an attempt to explore further the behavior of complex perovskite systems containing Ru(V), we prepared and characterized $\text{CaCu}_3\text{Ga}_2\text{Ru}_2\text{O}_{12}$. This composition was predicted by SPuDS (Structure Prediction Diagnostic Software) to be stable under high-pressure–high-temperature synthetic conditions.¹⁴ Recently, similar perovskites such as $\text{CaCu}_3\text{Ga}_2\text{M}_2\text{O}_{12}$ ($\text{M} = \text{Nb}$, Sb , and Ta) have been synthesized at high pressure.¹⁵ In those compounds, the six-coordinate sites are occupied by either d^0 or d^{10} cations. The main purpose of this paper is to report on the successful synthesis of the predicted ruthenate and to discuss its unusual metallic conductivity. To the best of our knowledge, $\text{CaCu}_3\text{Ga}_2\text{Ru}_2\text{O}_{12}$ is a rare example of metallic conductivity in a perovskite-type oxide containing Ru(V). This interesting behavior is thought to be associated with the large degree of electron transfer between Cu 3d and Ru 4d states.

Experimental Section

For the synthesis of $\text{CaCu}_3\text{Ga}_2\text{Ru}_2\text{O}_{12}$, appropriate stoichiometric mixtures of dried CaCO_3 , CuO , Ga_2O_3 , and RuO_2 were calcined at 900 °C in air for 8 h with intermittent grinding. The reacted oxide mixture was then thoroughly reground and sealed in a Au capsule with an inside diameter of 3.2 mm and a wall thickness of 0.1 mm. High-pressure–high-temperature (HPHT) reaction conditions were applied at 12.5 GPa and 1200 °C, followed by temperature quenching and slow decompression using the 2000 ton uniaxial split sphere apparatus (USSA 2000).¹⁶ The sample was then recovered from the Au capsule as a dense pellet with a volume of roughly 50 mm³. Details of the cell assembly along with the temperature and the pressure calibrations are described in the literature.^{17,18}

The formation of a perovskite-related phase was initially confirmed from an X-ray diffraction pattern, taken on the sample pellet after recovery from the HPHT reaction using a general area detector diffraction system (GADDS). All major peaks in the powder diffraction pattern could be indexed on the basis of a body-centered cubic cell with an approximate cell dimension $a \approx 7.44 \text{ \AA}$. Intensity data suitable for Rietveld structure refinement were collected on a MacScience model M18XHF diffractometer installed on a rotating anode X-ray source operating at 50 kV and 300 mA. Monochromatic $\text{Cu K}\alpha$ radiation was obtained using a curved crystal of graphite. The data were collected with a step-scan procedure in the range $2\theta = 10\text{--}90^\circ$ with a step width of 0.02° and a counting time of 1 s per step. The unit cell parameter was derived by least-squares refinement using the full powder diffraction pattern. Because of a limited quantity of sample recovered after the high-pressure treatment, the data were obtained for a small amount of powder sample dispersed on a glass plate with absolute ethanol. The background noise from a glass plate was removed by subtracting the data of the glass plate, producing an essentially flat background. The refinement of reflection positions and intensities was carried out using the Rietveld analysis program RIETAN-2000.¹⁹

Elemental analysis using the energy-dispersive X-ray (EDX) emission technique gave the stoichiometric composition within experimental error. Dc magnetic susceptibility measurement

for sample powder was carried out in the temperature range from 5 to 300 K in an applied magnetic field of 5 kG using a Quantum Design MPMS-5 SQUID magnetometer. Electrical resistivity was measured using a standard four-probe technique on the polycrystalline sample obtained directly as a dense pellet of about 86% density from the high-pressure synthesis. Data were collected in the temperature range 10–400 K in a closed-cycle helium cryostat.

Results and Discussion

Attempts to synthesize $\text{CaCu}_3\text{Ga}_2\text{Ru}_2\text{O}_{12}$ at ambient pressure were unsuccessful. Instead CaRuO_3 appears as the majority phase when the oxide mixture with the desired stoichiometry was subjected to ambient pressure heat treatments. The $\text{CaCu}_3\text{Ga}_2\text{Ru}_2\text{O}_{12}$ phase was isolated as the dominant phase only after temperature quenching the sample from high-pressure conditions.

The X-ray powder diffraction pattern of $\text{CaCu}_3\text{Ga}_2\text{Ru}_2\text{O}_{12}$ was quite similar to those obtained previously for $\text{CaCu}_3\text{Ga}_2\text{M}_2\text{O}_{12}$ ($\text{M} = \text{Nb}$, Sb , and Ta),¹⁵ thereby implying it is isostructural with those compounds. As observed in the $\text{M} = \text{Sb}$ and Ta members of this structural family, an ordering of the octahedral cations, Ga and M, in the $\text{a}^+\text{a}^+\text{a}^+$ tilt system changes the space group symmetry from $\text{Im}\bar{3}$ to $\text{Pn}\bar{3}$.²⁰ The appearance of the (111) peak in the X-ray diffraction pattern is a very sensitive indicator of the degree of ordering of cations over the octahedral sites (the B-sites). The absence of any intensity at the angle expected for the (111) reflection indicates that $\text{CaCu}_3\text{Ga}_2\text{Ru}_2\text{O}_{12}$ crystallizes in space group $\text{Im}\bar{3}$ with Ga and Ru randomly distributed over the available octahedral sites. This is different from the $\text{M} = \text{Sb}$ and Ta members of the $\text{CaCu}_3\text{Ga}_2\text{M}_2\text{O}_{12}$ family, where the M(V)/Ga(III) cations are ordered (at least partially), but is similar to the $\text{M} = \text{Nb}$ member. Considering that the present compound was prepared under high pressure, a possibility could be supposed that some of Cu(II) ions are on the octahedral sites along with complementary Ga(III) ions on the square planar sites. However, the good agreement between Ga(III) on the octahedral site and SPuDS predictions and no example of this structure type with non-Jahn–Teller ions on the square planar site do not support such a picture. Accordingly, the atomic positions of disordered perovskite $\text{CaCu}_3\text{Ga}_2\text{Nb}_2\text{O}_{12}$ were used in the initial stages of structure refinement for $\text{CaCu}_3\text{Ga}_2\text{Ru}_2\text{O}_{12}$. Weak additional peaks that are not indexed in either $\text{Im}\bar{3}$ or $\text{Pn}\bar{3}$ also appeared in the diffraction pattern. Multiple attempts to index the impurity peaks were unsuccessful, largely due to their low intensities. The positions of the impurity peaks did not correspond to X-ray patterns expected for likely minority phases, such as CaRuO_3 , Ca_2RuO_4 , RuO_2 , and both polymorphs of Ga_2O_3 . It should be noted that no systematic relationship was observed between the positions and intensities of these peaks and the positions and intensities expected to arise from a distortion of the perovskite structure to lower symmetry. In particular no peaks could be indexed at half-integral positions on the basis of either the a or $(\sqrt{2})a$ perovskite subcell. The impurity peaks were thus excluded from the refinement, which reduced the re-

(14) Lufaso, M. W.; Woodward, P. M. *Acta Crystallogr.* **2001**, *B57*, 725.

(15) Byeon, S.-H.; Lufaso, M. W.; Parise, J. B.; Woodward, P. M.; Hansen, T. *Chem. Mater.* **2003**, *15*, 3798.

(16) Liebermann, R. C.; Wang, Y. *High-Pressure Research: Application to Earth and Planetary Sciences*; Terrapub: Tokyo, 1992.

(17) Gwanmesia, G. D.; Li, B.; Liebermann, R. C. *PAGEOPH* **1993**, *141*, 467.

(18) Leinenweber, K.; Parise, J. B. *J. Solid State Chem.* **1995**, *114*, 277.

(19) Izumi, F.; Murata, H.; Watanabe, N. *J. Appl. Crystallogr.* **1987**, *20*, 411.

(20) Howard, C. J.; Kennedy, B. J.; Woodward, P. M. *Acta Crystallogr.* **2003**, *B59*, 463.

Table 1. Structure Refinement Results for $\text{CaCu}_3\text{Ga}_2\text{Ru}_2\text{O}_{12}$ ^a

atom	x	y	z	B (\AA^2)
Ca	0.0	0.0	0.0	0.49(6)
Cu	0.0	0.5	0.5	0.53(6)
Ga/Ru	0.25	0.25	0.25	0.84(9)
O	0.0	0.168(2)	0.308(2)	1.0 ^b

^a The space group is $Im\bar{3}$, the cell edge $a = 7.4306(8)$ \AA , and the goodness of fit parameters are $R_p = 0.1185$ and $R_l = 0.0788$.

^b Fixed value.

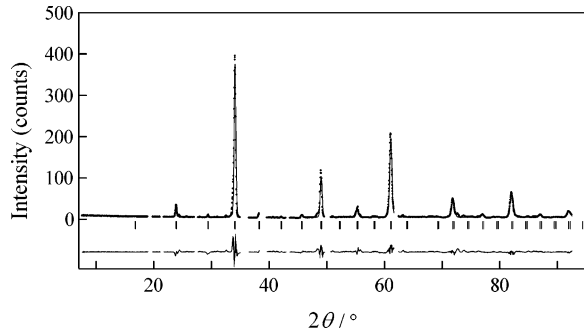


Figure 1. Observed X-ray powder diffraction data (dotted line) along with the calculated diffraction pattern (solid line) obtained from Rietveld refinement of $\text{CaCu}_3\text{Ga}_2\text{Ru}_2\text{O}_{12}$. Regions of the pattern containing impurity peaks are excluded. At the bottom of the figure the difference plot ($I_{\text{obsd}} - I_{\text{calcd}}$) is shown on the same scale. Vertical bars on the bottom indicate the positions of allowed Bragg reflections.

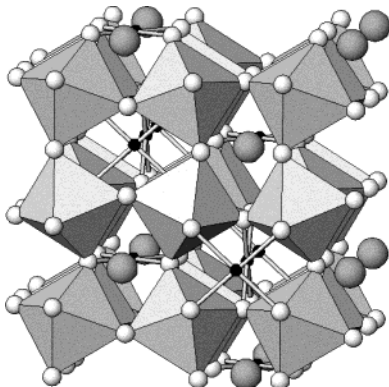


Figure 2. Idealized structure of $\text{CaCu}_3\text{Ga}_2\text{Ru}_2\text{O}_{12}$. Tilting of the octahedral network produces a square planar coordination for Jahn–Teller Cu(II) cations. Ga and Ru are statistically distributed over octahedral sites. Large spheres and small black spheres represent Ca and Cu atoms, respectively. Cu–O bonds in four-coordinated CuO_4 arrangement are represented.

sidual fit parameter noticeably. The isotropic displacement parameter of oxygen was fixed to 1.0 \AA^2 in the final stage of refinement since the refinement of individual atomic temperature factors gave a negative value for the oxygen atom.

Crystallographic data, including refined atomic coordinates and isotropic displacement parameters, are listed in Table 1. The observed, calculated, and difference profiles from the Rietveld refinement of $\text{CaCu}_3\text{Ga}_2\text{Ru}_2\text{O}_{12}$ are plotted in Figure 1. As shown in Figure 2, the idealized structure of $\text{CaCu}_3\text{Ga}_2\text{Ru}_2\text{O}_{12}$ is quite similar to that of $\text{CaCu}_3\text{Ti}_4\text{O}_{12}$,^{22,23} where the Ti

sites are replaced with an equal ratio of Ga and Ru in a disordered manner. Selected bond distances and angles for $\text{CaCu}_3\text{Ga}_2\text{Ru}_2\text{O}_{12}$ are compared to those of other members of the $\text{CaCu}_3\text{Ga}_2\text{M}_2\text{O}_{12}$ and $\text{CaCu}_3\text{M}_4\text{O}_{12}$ family in Table 2. The unit cell dimension determined from Rietveld refinement, $a = 7.4306(8)$ \AA , is significantly smaller than those determined previously, 7.4701, 7.4483, and 7.4663 \AA for $\text{CaCu}_3\text{Ga}_2\text{Nb}_2\text{O}_{12}$, $\text{CaCu}_3\text{Ga}_2\text{Sb}_2\text{O}_{12}$, and $\text{CaCu}_3\text{Ga}_2\text{Ta}_2\text{O}_{12}$, respectively. If we consider the ionic radii, $r(\text{Nb}^{5+}) = 0.64 \text{ \AA}$, $r(\text{Sb}^{5+}) = 0.60 \text{ \AA}$, $r(\text{Ta}^{5+}) = 0.64 \text{ \AA}$, $r(\text{Ru}^{4+}) = 0.62 \text{ \AA}$, and $r(\text{Ru}^{5+}) = 0.565 \text{ \AA}$,²⁴ the more contracted unit cell size for $\text{CaCu}_3\text{Ga}_2\text{Ru}_2\text{O}_{12}$ strongly suggests that the majority of Ru ions are in the +5 oxidation state rather than +4 state. The (Ga/Ru)–O–(Ga/Ru) angles are reduced to 136.2° by the (Ga/Ru)O₆ octahedral tilts, producing a square planar coordination for the Cu(II) cation. Actually this square planar site shows a slight rectangular distortion, and there are four oxygen atoms in the second coordination sphere at a distance of 2.85 \AA .

One of the more interesting features of the $\text{CaCu}_3\text{Ga}_2\text{Ru}_2\text{O}_{12}$ structure is the short Cu–O bond length (1.895 \AA). This bond length is markedly shorter than observed in the other compounds in Table 2. The empirical expression for the bond valence, $v_{ij} = \exp[(R_{ij} - d_{ij})/b]$, where R_{ij} and d_{ij} are the bond valence parameter and bond length, has been widely adopted to estimate valences in inorganic solids.²⁵ The bond valence sums for the copper ion ($R_{ij} = 1.679 \text{ \AA}$, $b = 0.37 \text{ \AA}$) are 2.07, 2.03, 2.06, and 2.31 in $\text{CaCu}_3\text{Ga}_2\text{Sb}_2\text{O}_{12}$, $\text{CaCu}_3\text{Ga}_2\text{Ta}_2\text{O}_{12}$, $\text{CaCu}_3\text{Ga}_2\text{Nb}_2\text{O}_{12}$, and $\text{CaCu}_3\text{Ga}_2\text{Ru}_2\text{O}_{12}$, respectively. The first three compounds have Cu bond valence sums similar to that of $\text{CaCu}_3\text{Ti}_4\text{O}_{12}$ (1.99), while the copper coordination environments in $\text{CaCu}_3\text{Ga}_2\text{Ru}_2\text{O}_{12}$ and $\text{CaCu}_3\text{Ru}_4\text{O}_{12}$ (2.20) suggest significant oxidation of Cu(II). In both structures the only ion capable of oxidizing copper is ruthenium.

The magnetic susceptibility of $\text{CaCu}_3\text{Ga}_2\text{Ru}_2\text{O}_{12}$ as a function of temperature (Figure 3) appears to exhibit a temperature-independent Pauli-paramagnetic behavior. Neither magnetic ordering nor Curie–Weiss paramagnetism was observed in the measured temperature range (5–300 K). It is instructive to compare and contrast this behavior with that of other $\text{A}_{1-x}\text{A}'_x\text{MRuO}_6$ perovskites. $\text{CaCu}_3\text{Ti}_4\text{O}_{12}$ antiferromagnetically orders below 27 K.²⁶ A calculation of the magnetic interactions in $\text{CaCu}_3\text{Ti}_4\text{O}_{12}$ suggested that antiferromagnetic order results from superexchange between (111) Cu–O planes. Another relevant compound is $\text{CaCu}_3\text{Mn}_4\text{O}_{12}$, which contains Mn(IV) (3d³) ions that are isoelectronic with Ru(V) (4d³). This compound shows large magnetoresistance behavior.²⁷ Disordered A_2MRuO_6 perovskites containing a mixture Ru(V) and a 3d-transition-metal ion, M, on the octahedral sites (i.e., $\text{Sr}_2\text{FeRuO}_6$ and BaLaNiRuO_6)¹¹ do not

(23) Subramanian, M. A.; Sleight, A. W. *J. Solid State Chem.* **2002**, *4*, 347.

(24) Shannon, R. D. *Acta Crystallogr.* **1976**, *A32*, 751.

(25) Brown, I. D. *The Chemical Bond in Inorganic Chemistry. The Bond Valence Model*; IUCr Monograph on Crystallography, Vol. 12; Oxford University Press: Oxford, 2002.

(26) Collomb, A.; Samaras, D.; Bochu, B.; Joubert, J. C. *Phys. Status Solidi A* **1977**, *41*, 459.

(27) Zeng, Z.; Greenblatt, M.; Subramanian, M. A.; Croft, M. *Phys. Rev. Lett.* **1999**, *82*, 3164.

(21) Subramanian, M. A.; Sleight, A. W. *Solid State Sci.* **2002**, *4*, 347.

(22) Bochu, B.; Deschizeaux, M. N.; Jubert, J. C.; Collomb, A.; Chenavas, J.; Marezio, M. *J. Solid State Chem.* **1979**, *29*, 291.

Table 2. Structure Parameters for $\text{CaCu}_3\text{Ga}_2\text{Ru}_2\text{O}_{12}$ and Related $\text{CaCu}_3\text{M}_2\text{M}'_2\text{O}_{12}$ and $\text{CaCu}_3\text{M}_4\text{O}_{12}$ Compounds

M/M	Ru/Ga	Sb/Ga ¹⁵	Ta/Ga ¹⁵	Nb/Ga ¹⁵	Ru ²¹	Ti ²¹
<i>a</i> (Å)	7.4306(8)	7.4483(4)	7.4663(2)	7.4701(4)	7.428(1)	7.4037(5)
space group	<i>Im</i> 3	<i>Pn</i> 3	<i>Pn</i> 3	<i>Im</i> 3	<i>Im</i> 3	<i>Im</i> 3
bond distances (Å)						
Ca–O (12)	2.609(4)	2.6274(7)	2.6323(8)	2.66(1)	2.628(2)	2.608(1)
Cu–O (4)	1.895(3)	1.9691(6)	1.9764(7)	1.96(1)	1.934(2)	1.978(1)
M/M–O (6)	2.002(4)	1.980(2) ^a	1.984(6) ^a	1.989(4)	1.9848(7)	1.9625(4)
bond angles (deg)						
O–Cu–O (2)	82.5(8)	84.65(4)	84.61(5)	86.0(4)	84.5(1)	84.68(6)
O–Cu–O (2)	97.5(8)	95.36(4)	95.39(5)	94.0(4)	95.5(1)	95.32(6)
O–M/M–O (6)	89.1(6)	89.61(3)	89.59(3)	89.3(4)	89.93(7)	89.44(4)
O–M/M–O (6)	90.9(6)	90.39(3)	90.41(3)	90.7(4)	90.07(7)	90.56(4)
M/M–O–M/M	136.2(6)	140.26(3)	140.40(4)	139.7(5)	138.66(9)	141.33(6)

^a This distance is an average of the Ga and Sb/Ta sites. In $\text{CaCu}_3\text{Sb}_2\text{Ga}_2\text{O}_{12}$, the Sb–O distance is 1.961(1) Å and the Ga–O distance is 1.999(2) Å. In $\text{CaCu}_3\text{Ta}_2\text{Ga}_2\text{O}_{12}$, the Ta–O distance is 1.986(6) Å and the Ga–O distance is 1.981(6) Å.

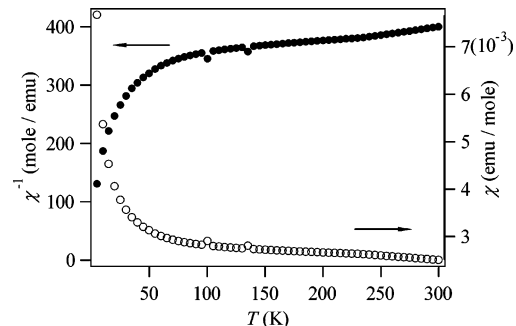


Figure 3. Temperature dependence of the magnetic susceptibility for $\text{CaCu}_3\text{Ga}_2\text{Ru}_2\text{O}_{12}$.

magnetically order. The lack of cation order leads to frustration that prevents long-range magnetic order, but this stabilizes spin-glass behavior rather than Pauli paramagnetism. Ordered ruthenium(V) oxides (i.e., $\text{Sr}_2\text{LuRuO}_6$,²⁸ Ba_2YRuO_6 ,²⁸ $\text{Ba}_2\text{LuRuO}_6$,²⁸ BaLaZnRuO_6 ,¹¹ $\text{Ca}_2\text{NdRuO}_6$,⁹ $\text{Ca}_2\text{HoRuO}_6$,⁹ $\text{Sr}_2\text{ErRuO}_6$,⁹ $\text{Ba}_2\text{LaRuO}_6$,²⁹ and $\text{Ca}_2\text{LaRuO}_6$ ²⁹) generally undergo antiferromagnetic ordering at low temperature where the dominant magnetic coupling is π -superexchange interactions via Ru(V)–O–O–Ru(V) pathways. There are several features of the magnetic properties of these compounds that differ from the behavior expected for a typical antiferromagnet. Battle, Goodenough, and Price suggested that the behavior of these compounds can be understood by assuming partial delocalization of Ru t_{2g} electrons through Ru(V)–O–O–Ru(V) pathways.²⁹ However, it should be noted that neither Pauli paramagnetism nor metallic conductivity is observed. The question of localized vs itinerant electrons was probably best summarized by Battle and Jones, who suggest that the magnetic properties are consistent with a d-electron system that has moved out of the localized regime and yet is not completely delocalized.²⁸ Clearly the magnetic properties of $\text{CaCu}_3\text{Ga}_2\text{Ru}_2\text{O}_{12}$ are distinctly different. Therefore, we propose that the Pauli-paramagnetic behavior observed in $\text{CaCu}_3\text{Ga}_2\text{Ru}_2\text{O}_{12}$, where the magnetic Ru ions and the d¹⁰ diamagnetic Ga ions are randomly distributed over the octahedral sites, can be attributed to a delocalization mechanism involving both CuO_4 square planes and RuO_6 octahedra.

Temperature-dependent electrical resistivity data in Figure 4 show that $\text{CaCu}_3\text{Ga}_2\text{Ru}_2\text{O}_{12}$ is metallic, con-

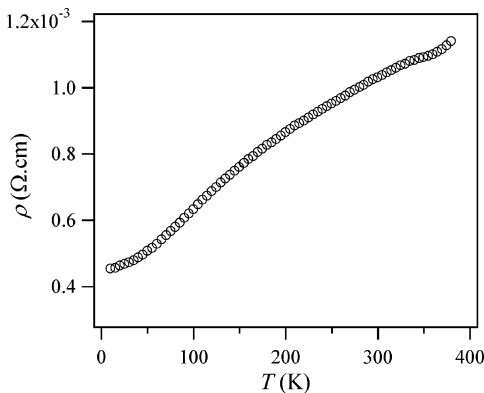


Figure 4. Temperature dependence of the resistivity for $\text{CaCu}_3\text{Ga}_2\text{Ru}_2\text{O}_{12}$.

sistent with the measured magnetic data. Itinerant electron transport is also observed for the ruthenium(IV) oxide $\text{CaCu}_3\text{Ru}_4\text{O}_{12}$.⁶ Considering the diluted Ru concentration and the filled d-orbital of Ga, it is interesting that the electrical resistivity ($\sim 1 \times 10^{-3} \Omega \cdot \text{cm}$ at room temperature) of $\text{CaCu}_3\text{Ga}_2\text{Ru}_2\text{O}_{12}$ is comparable to that of $\text{CaCu}_3\text{Ru}_4\text{O}_{12}$ ($\sim 8 \times 10^{-4} \Omega \cdot \text{cm}$ at room temperature). It is generally accepted that the contrasting electrical and magnetic properties of CaRuO_3 and SrRuO_3 depend on the Ru–O–Ru bond angle, thought to be crucial for Ru 4d–O 2p orbital overlap. On the basis of this logic, the strongly distorted Ru–O–Ru angle (139°) seen in $\text{CaCu}_3\text{Ru}_4\text{O}_{12}$ should give rise to a magnetic semiconductor. Therefore, the metallic behavior of $\text{CaCu}_3\text{Ru}_4\text{O}_{12}$ can only be attributed to Ru/Cu valence degeneracy of some type.²¹ The lack of localized magnetic moments on either Cu or Ru coupled with the bond valence calculations indicates that there are both Cu 3d and Ru 4d states at the Fermi level of $\text{CaCu}_3\text{Ru}_4\text{O}_{12}$. Valence degeneracy has been investigated in the double perovskites Ba_2FeMO_6 (M = Mo and Re), where the oxidation states of Fe(III) + M(V) on the octahedral sites are considered to be degenerate with the Fe(II) + M(VI) state combination.³⁰ If we note that the average Ga/Ru–O–Ga/Ru angle is significantly distorted to 136.2° (Table 2), the metallic character of $\text{CaCu}_3\text{Ga}_2\text{Ru}_2\text{O}_{12}$ is likely to have an origin similar to that of the metallicity observed in $\text{CaCu}_3\text{Ru}_4\text{O}_{12}$. While the dilution of ruthenium on the octahedral sites would be expected to reduce the conductivity somewhat, the presence of ruthenium that is formally Ru(V) rather

(28) Battle, P. D.; Jones, C. W. *J. Solid State Chem.* **1989**, *78*, 108.

(29) Battle, P. D.; Goodenough, J. B.; Price, R. *J. Solid State Chem.* **1983**, *46*, 234.

(30) Sleight, A. W.; Weiher, J. F. *J. Phys. Chem. Solids* **1972**, *33*, 679.

than Ru(IV) should increase its oxidizing power, thereby enhancing the $\text{Cu}(\text{II})-\text{O}-\text{Ru}(\text{V}) \leftrightarrow \text{Cu}(\text{III})-\text{O}-\text{Ru}(\text{IV})$ charge transfer.

In conclusion we have successfully synthesized $\text{CaCu}_3\text{Ga}_2\text{Ru}_2\text{O}_{12}$ under high-pressure and high-temperature conditions. The Ga and Ru atoms in the perovskite-like structure are disordered over the octahedral sites. The Cu–O bonds are considerably shorter than expected for square planar Cu(II). Magnetic susceptibility and electrical transport measurements show that $\text{CaCu}_3\text{Ga}_2\text{Ru}_2\text{O}_{12}$ is a Pauli-paramagnetic conductor. All observations indicate that the unusual proper-

ties of $\text{CaCu}_3\text{Ga}_2\text{Ru}_2\text{O}_{12}$ originate from a valence degeneracy between $\text{Cu}(\text{II}) + \text{Ru}(\text{V})$ and $\text{Cu}(\text{III}) + \text{Ru}(\text{IV})$.

Acknowledgment. J.B.P. thanks the NSF through its DMR and EAR programs for support. S.-H.B. thanks the NSF for support during the stay at Stony Brook. P.M.W. thanks the NSF-DMR program for support. Research carried out at Kyung Hee University was supported by KOSEF Grant R01-2001-000-00045-0.

CM049265T